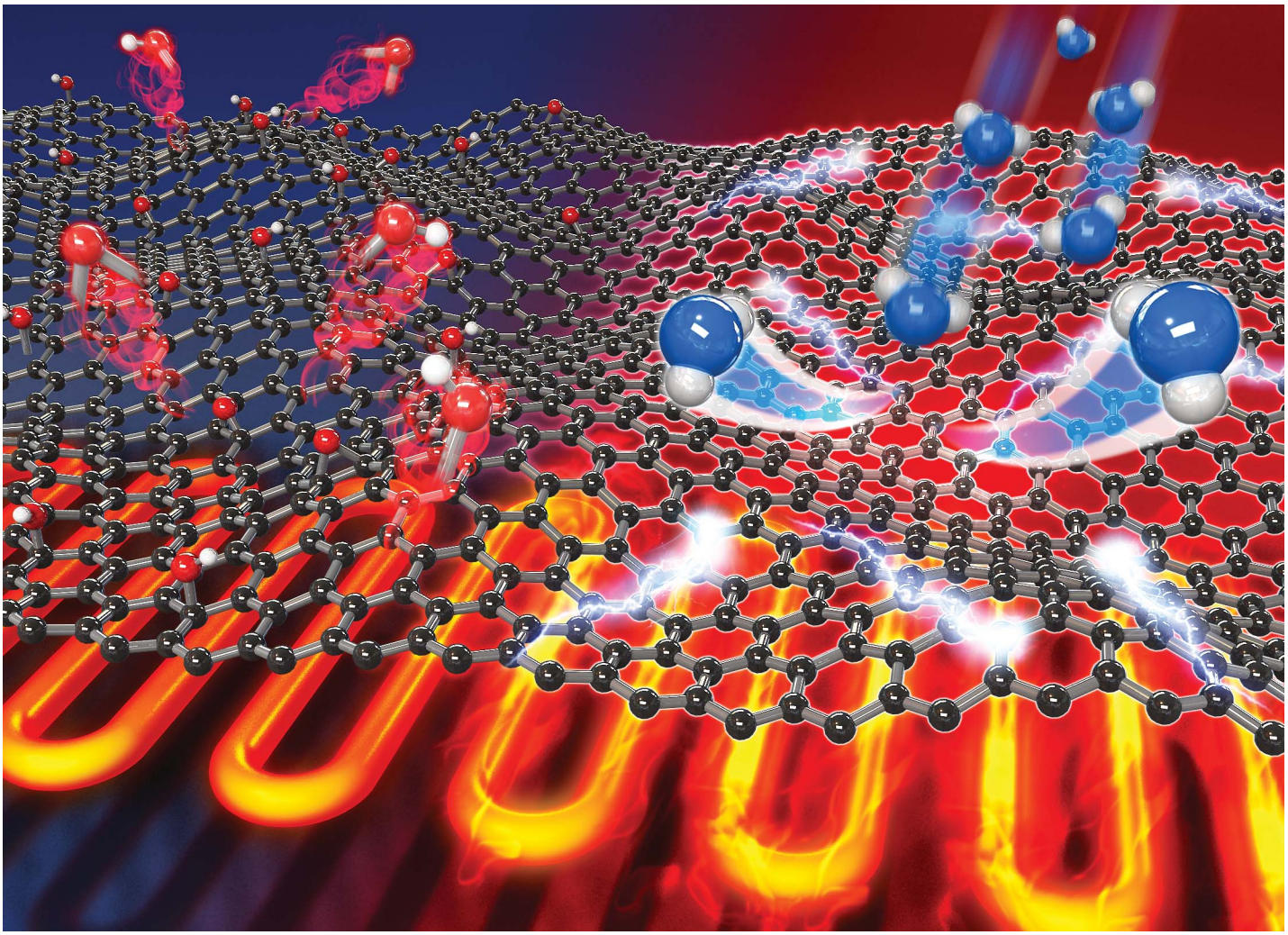

Showcasing research from Professor Han's laboratory, Department of Electro-Functionality Materials, University of Science and Technology (KERI campus), Changwon, South Korea.

Extraordinary thermal behavior of graphene oxide in air for electrode applications

The thermal stability of graphene oxide (GO) in air is one of the most important physical properties influencing its potential applications. GO having functional groups, such as carboxyl and lactol groups that possess defective basal plane structures is unstable in air. This study demonstrates that less defective and metal ion-free GO nanosheets with a high oxidation level can remain very stable even above 300 °C under ambient conditions. The superior thermal stability of our GO is favorable for the fabrication of conductive graphene films and fibers by low-temperature annealing.

As featured in:

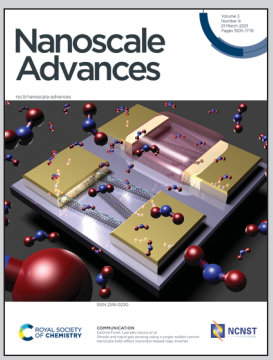

See Joong Tark Han *et al.*, *Nanoscale Adv.*, 2021, **3**, 1597.

ROYAL SOCIETY OF CHEMISTRY

rsc.li/nanoscale-advances

Registered charity number: 207890

Nanoscale Advances

ROYAL SOCIETY OF CHEMISTRY

PAPER

View Article Online
View Journal | View Issue

Cite this: *Nanoscale Adv.*, 2021, **3**, 1597

Extraordinary thermal behavior of graphene oxide in air for electrode applications†

Joon Young Cho,[ab] Jung Hoon Kim[a] and Joong Tark Han *[ab]

The thermal stability of solution-exfoliated graphene oxide (GO) in air is one of the most important physical properties influencing its potential applications. To date, the majority of the GO prepared by the $KMnO_4$-based oxidation of graphite is thermally unstable in air due to the presence of highly oxidative functional groups, such as carboxyl and lactol groups that possess defective basal plane structures. Here, we demonstrate that less defective and metal ion-free GO nanosheets including those with a high oxidation level can remain very stable even above 300 °C under ambient conditions. These GO nanosheets were produced by the exfoliation of graphite oxide fabricated by the modified Brodie method in NH_4OH solution, effectively excluding metal ions that can promote the thermal decomposition of GO in air at elevated temperatures. The deoxygenation of ammonia-assisted GO (AGO) was initiated at temperatures above 200 °C, while GO exfoliated in the KOH solution (KGO) decomposed, even at 180 °C. Notably, AGO was exceptionally resistant at 400 °C, even at a very slow heating rate of 2 °C min^{-1}. Conversely, KGO was significantly oxidized, even at 250 °C. The superior thermal stability of AGO is favorable for the fabrication of conductive surface graphene films and conductive fibers by low-temperature annealing.

Received 30th September 2020
Accepted 1st January 2021

DOI: 10.1039/d0na00805b

rsc.li/nanoscale-advances

Introduction

Graphene oxide (GO)—produced *via* the oxidation of graphite powder—has been extensively investigated for use in electrodes, templates for hybrid materials, and interfacial modifiers owing to its solution processability.[1–4] The fabrication of electrically and thermally conductive graphene nanosheets requires GO to be deoxygenated by thermal, photothermal, chemical, and electrochemical approaches. The thermal deoxygenation of GO following its deposition on target substrates is one of the most economical reduction processes. However, GO with highly oxidative functional groups is susceptible to air, even at low temperatures (<350 °C). This vulnerability is due to the fact that the O_2 molecules in air facilitate the decomposition of sp^2 carbon atoms, leading to the evolution of CO and CO_2 by decomposition of the C–C bonds.[5,6] Moreover, the oxidation of graphite powder with strong oxidants such as $KMnO_4$ can generate permanent defects, including partial cleavage of hexagonal sp^2-hybridized crystalline structures (Fig. 1a). These defects are significantly disadvantageous for the production of highly crystalline graphene from GO.[7] To prevent the rupture of the hexagonal sp^2 carbon structure, several synthetic protocols for graphite oxide have been reported in which $KMnO_4$ is still used as the oxidant.[8] However, it is difficult to prevent the formation of highly oxidative functional groups such as carboxylic acid or lactol groups that are difficult to remove from the GO surface or edges at low temperature.[9]

The oxidation of graphite by the Brodie method, which uses chlorate compounds as the oxidant, is an alternative method for minimizing the formation of permanent defective structures and highly oxidative functional groups (Fig. 1b).[10] However, the interlayer *d*-spacing of graphite oxide (GPO) fabricated by chlorate-based oxidation is considerably smaller than that of

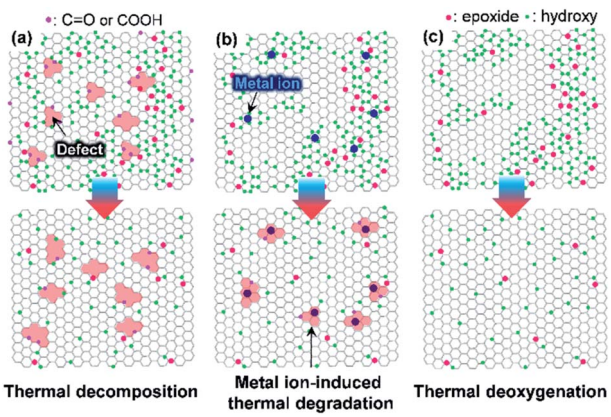

Fig. 1 Possible structures of GO depending on oxidation and exfoliation methods. GO (a) with permanent defects, (b) without permanent defects but with metal ions, and (c) without permanent defects and metal ions and with epoxide and hydroxyl groups.

[a]*Nano Hybrid Technology Research Center, Korea Electrotechnology Research Institute (KERI), Changwon 51543, Republic of Korea. E-mail: jthan@keri.re.kr*

[b]*Department of Electro-Functionality Materials Engineering, University of Science and Technology (UST), Changwon 51543, Republic of Korea*

† Electronic supplementary information (ESI) available: FE-SEM images, TGA, UV-vis spectra and results of WVTR. See DOI: 10.1039/d0na00805b

$KMnO_4$-based GPO (>8 Å) due to the formation of less highly oxidative carboxylic acid groups.[10,11] Thus, additional chemical or physical forces must be applied to exfoliate GPO into a single-layer GO in aqueous solutions.[12] Generally, alkaline solutions such as aqueous KOH and NaOH solutions were used to exfoliate GPO.[13,14] However, this allows alkali metal impurities to be retained by adsorption on oxidative functional groups of GO or sp^2 carbon structures, which can have a detrimental effect on the thermal stability of GO in air.[15] In this context, if GO is produced with a less defective structure and a high thermal stability, as illustrated in Fig. 1c, the applicability of graphene derived from GO can be extended. For example, such graphene may be used for the deposition of graphene films on plastic substrates at low temperatures or for interfacial functional layers for flexible electrodes or optoelectronic devices, respectively. This can result in the fabrication of high gas barrier layers on flexible polymer substrates that are essential for flexible devices such as rollable displays.

Herein, we demonstrate that GO nanosheets with less defective structures and lower metal ion impurity content are thermally stable in air, even at 400 °C. This was achieved by exfoliating less defectively oxidized graphite oxide in ammonia solution using a high-speed homogenizer to apply the shear stress in solution.[16] The ambient thermal deoxygenation behavior of GO was monitored by Raman spectroscopy, X-ray photoelectron spectroscopy (XPS), and thermogravimetric analysis-mass spectrometry (TGA-MS). Moreover, the swelling behavior and electrical properties of thermally stable GO films were investigated before and after thermal deoxygenation in air.

Experimental

Materials

Pure graphite powder (99.999% purity, −200 mesh), $NaClO_3$ powder, and fuming nitric acid were purchased from Alfa Aesar, Samchun Chemicals, and TCI Chemicals, respectively. HCl, H_2O_2, ammonium solution, acetone, and ethanol were obtained from Daejung Chemicals and Metals Co., Ltd. and used without further treatment. KOH powder was purchased from Sigma-Aldrich.

Fabrication of graphite oxide powder and GO dispersion

A less defective GO was fabricated by oxidizing graphite into GPO using a ClO_3-based oxidation method, *i.e.*, by kneading the premixed graphite/$NaClO_3$ powder with fuming HNO_3 to reduce the oxidation time and the amount of acid waste, as previously reported.[17] First, graphite powder (10 g) was mixed with $NaClO_3$ powder (75 g) and the mixed powder was placed and leveled on the base of a crystallizing dish. The weight ratio of graphite to $NaClO_3$ remained fixed at 1 : 7.5 (w/w), and the oxidation time of graphite was varied to control the degree of graphite oxidation. Next, fuming nitric acid (100 mL) was poured slowly while kneading it into the mixed powder; the mixture was allowed to rest for 2 or 3 h at room temperature (GPO1, GPO2). Deionized (DI) water was used to quench the oxidation reaction, and HCl and H_2O_2 were subsequently added to remove the metal ions and impurities. Finally, GPO, which is naturally acidic, was neutralized with DI water and freeze-dried. GPO3 was prepared by repeating the aforementioned process once more. The synthesized GPO powder was immersed into aqueous KOH and ammonium solution at pH 11 at 1 g L^{-1} concentration. To exfoliate a few layers of the GO sheets, a high-speed homogenizer was used at 8000 rpm for 1 h. The GO dispersion was centrifuged at 10 000 rpm for 1 h to obtain the GO dopant for the fibers.

Fabrication and thermal treatment of AGO films and fibers

The GO films were fabricated by solution casting. The GO solution (10 mL) was cast on the polystyrene square dish, and allowed to rest for a week. After the GO films were dried, the films were detached and dried at 80 °C for 1 h. The GO films on PI were fabricated using an air spray coater (NCS200) with 500 mg L^{-1} GO solutions. The GO fibers were prepared by wet spinning. The GO dopant (1.4 wt%) was filled into a syringe and pressed overnight for degassing. The prepared GO dopant was injected into a rotating acetone bath through a 23 G needle at 5.6 m min^{-1}. The wet fibers were drawn out vertically and dried on a Teflon bobbin under an infrared lamp. The GO films and fibers were annealed in a convection oven at 150, 175, 200, 225, and 250 °C for 1 h at a ramping rate of 2 °C min^{-1}.

Characterization

The crystalline structure of the GPO powder and the *d*-spacing of the AGO films were characterized by X-ray diffraction (XRD) using a Philips PW 3830 X-ray diffractometer with Cu Kα radiation ($\lambda = 1.5418$ Å). The ratio of the functional groups of GPO and GO was identified by XPS using a K-Alpha+ system (Thermo Fisher Scientific, U.K.) spectrometer with monochromated Al K-α X-ray radiation as the X-ray excitation source and ^{13}C solid-state nuclear magnetic resonance (^{13}C NMR) spectroscopy (AVANCE II+ 400 MHz, Bruker). The morphology of GO sheets and GO fibers was imaged by field-emission scanning electron microscopy (FE-SEM) (HITACHI S4800) and atomic force microscopy (AFM) using a Bruker nanoscope multimode system in the tapping mode. The structural characteristics of GPO were confirmed by Raman spectrometry (NTEGRA, NT-MDT) at an excitation wavelength of 532 nm. UV-vis spectra were obtained using a UV-vis spectrometer (Agilent, Varian Cary 5000). The thermal behaviors of GO were analyzed by TGA (TA Instruments, TGA Q500) in air at a ramping rate of 2 °C min^{-1} and TGA-MS (STA 409 PC/QMS 4003C, NETZCH) in an Ar atmosphere at a ramping rate of 2 °C min^{-1}. The electrical characteristics of the thermally treated GO films and fibers were investigated using a two-probe resistivity measuring instrument with a 50 μm spacing. The water vapor transmission rates (WVTR) of the GO films on PI films were measured using a MOCON Permatran W 3/33 MA instrument.

Results and discussion

The oxidation level of GPO depends on the amount of the oxidant, the oxidation time, and the temperature. In this study,

to reduce the oxidation time and the amount of acid waste, the ground graphite/$NaClO_3$ powder mixture was reacted by adding a small amount of fuming nitric acid, followed by kneading and resting under ambient conditions. Fig. 2a depicts the XRD patterns of GPO powders obtained by varying the oxidation time. GPO prepared from graphite with a lateral size of >75 μm by oxidation for 2 h (GPO1) still exhibited (002) graphite peaks at 26°, corresponding to an interlayer spacing of 3.35 Å (Fig. 2a). The GPO peak generated at 15.5° corresponds to 5.7 Å (Fig. 2a). This is not sufficient for exfoliation, even in the aqueous alkaline solution (Fig. 2b). The *d*-spacing of GPO was increased by increasing the oxidation time to 3 h (GPO2). Thereafter, the characteristic graphite at 26° disappeared, while the *d*-spacing of GPO2 increased to 5.8 Å. This observation is indicative of the fact that at fixed concentrations of the oxidant, increased oxidation time can promote oxidation toward the in-plane direction by the diffusion of the oxidant molecules through the graphitic layers, as illustrated in Fig. 2b. GPO2 was exfoliated to produce GO with a strong base solution containing KOH (KGO) (Fig. S1a†). However, if a weak base solution containing ammonia (NH_4OH) is used to exclude the presence of metal ions, additional oxidative functional groups such as hydroxyl and epoxide should form on the basal plane because the pK_b value of ammonia (4.5) is much larger than that of KOH (0.5). Moreover, the electron affinity of the ammonium ion is smaller than that of the potassium ion. Actually, GPO2 was not completely exfoliated in aqueous NH_4OH (Fig. S1b†). To overcome this weak chemical force of NH_4OH, a new graphite oxide (GPO3) was fabricated in a stepwise oxidation manner; in each step, 2 h oxidation was conducted *via* a kneading-assisted process. The interlayer spacing of GPO3 was then increased to 6.41 Å. The full width at half-maximum of the (001) XRD peak for GPO3 (1.09) is significantly larger than that for GPO2 (0.54). This broadening of the *d*(001) plane in the XRD pattern shows that the *d*-spacing of the GPO edge is larger than that at the center, as illustrated in Fig. 2b. XPS data were obtained to assess the functional groups in GPO3. The C/O ratio from the survey scan in XPS was increased gradually from 3.3 (GPO1) to 4.35 (GPO3). The ^{13}C solid NMR spectrum of GPO3 shows that the C–O bonds from the hydroxyl and epoxy groups were mainly generated after oxidation (Fig. 2d).

This newly synthesized GPO3 was exfoliated to GO in an aqueous solution by adjusting the pH to 11 with NH_4OH, and is denoted as AGO. Importantly, to minimize the defect formation during mechanical exfoliation, shear stress in the solution that is applied using the high-speed homogenizer can provide sufficient force for GPO exfoliation in the presence of NH_4^+ and OH^-. FE-SEM (Fig. 2e) and AFM (Fig. 2f) images and the AFM height profile of AGO clearly exhibit the completely exfoliated single layer GO nanosheets with a thickness of 1 nm. The lateral size of AGO was determined to be 1–20 μm from the FE-SEM image in Fig. 2e. In addition, the ultraviolet-visible (UV-vis)

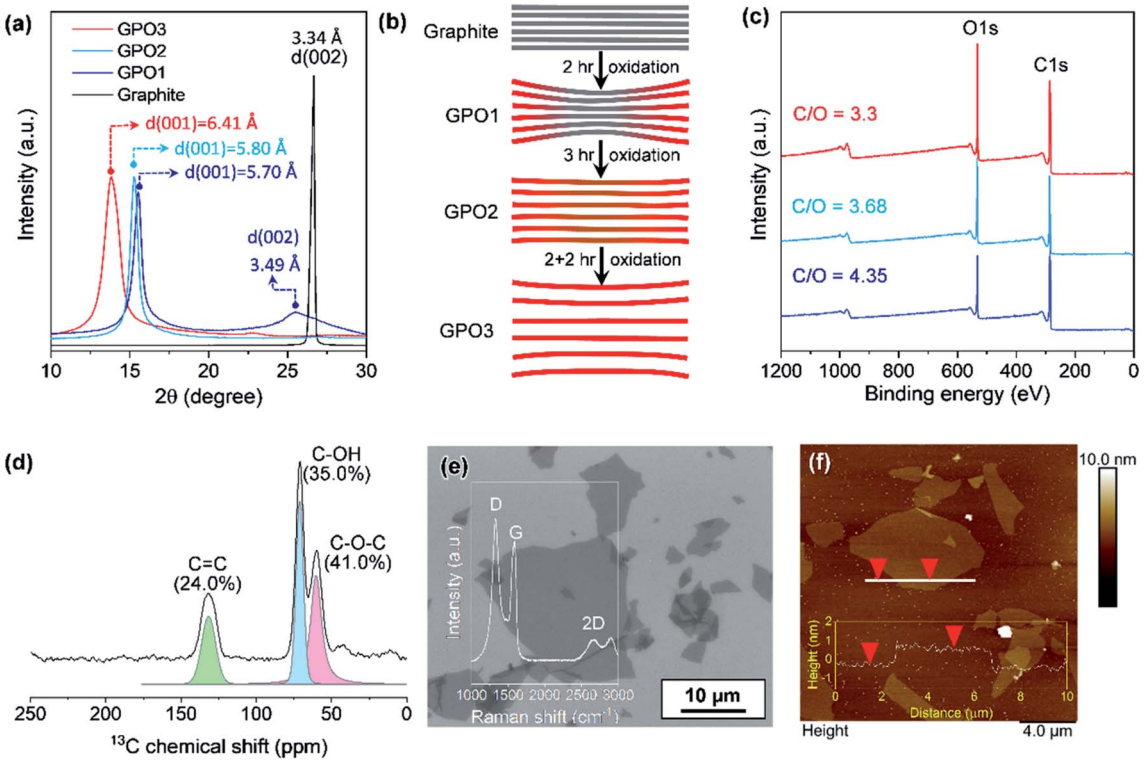

Fig. 2 (a) XRD spectra of GPO1 (2 h oxidation), GPO2 (3 h oxidation), and GPO3 (2 + 2 h oxidation). (b) Schematic representation of the *d*-spacing of graphite increased by varying the oxidation time and step. (c) XPS survey spectrum of GPO1, GPO2, and GPO3. (d) ^{13}C solid NMR spectrum of GPO3. (e) FE-SEM and (f) AFM images of exfoliated GPO3 in the aqueous NH_4OH solution. Insets in (e) and (f) depict the Raman spectrum and the height profile of a single layer GO on the Si wafer, respectively.

absorption spectra of the KGO and AGO dispersions in water (Fig. S2†) revealed strong peaks from the π–π* transitions of the C–C and C=C bonds in sp^2-hybridized regions, and the n–π* transition of the C–O bonds. Notably, distinct absorption peaks (>300 nm) corresponding to a typical polycyclic aromatic hydrocarbon skeleton were observed,[18] revealing that the synthesized GO contained large sp^2 domains even after harsh oxidation, corresponding to the images presented in Fig. 1b.

As illustrated in Fig. 1, the thermal stability of GO can be influenced by the existence of permanent defects generated during either the oxidation of graphite or the exfoliation of GPO by mechanical forces, and metal ions that can be incorporated during the oxidation or into an exfoliation medium such as the KOH solution. The XPS spectrum of exfoliated GPO3 in the aqueous KOH solution (KGO) in Fig. 3b shows that potassium ions (K^+) at 292.6 (K $2p_{3/2}$) and 295.4 eV (K $2p_{1/2}$) existed in the sample because K^+ can interact with oxidative functional groups and sp^2 domains. In stark contrast, XPS analysis revealed that no metal ions were detected in the AGO exfoliated in the ammonia solution (Fig. 3a).

The thermal stability of our synthesized AGO and KGO was then investigated by conducting the TGA in air at a very slow ramping rate of 2 °C min^{-1}. The AGO samples produced by our oxidation method caused explosions when heated, even at a heating rate of 3 °C min^{-1} (Fig. S3†). This means that our synthesized GO nanosheets have less defective structures, as illustrated in Fig. 1c. Fig. 3c shows the characteristic TGA thermograms of AGO and KGO in air. The detachment of the oxidative functional groups of KGO commenced at 150 °C, while the thermal deoxygenation of AGO started at 175 °C, which means that K^+ ions promote deoxygenation at low temperature. However, the weight loss of AGO was more dramatic than that of KGO, even at a very slow heating rate of 2 °C min^{-1}, as shown in the derivative thermogravimetry plot in Fig. 3c. This result is in stark contrast to that of the GO synthesized by the $KMnO_4$-based oxidation of graphite (Fig. S4a†). This corresponds to the fact that the GO synthesized by chlorate-based oxidation consists primarily of hydroxyl and epoxy groups, which can be detached from the GO surface more readily than the highly oxidative carboxylic acid or carbonyl groups. Furthermore, AGO was thermally stable, even at 400 °C. In contrast, KGO was thermally decomposed, even at 300 °C, which is due particularly to the leftover K^+ ions on the GO surface, as shown in the XPS spectrum (Fig. 3b). Notably, these results reveal that GO with less defective basal plane structures and without metal ions can be thermally reduced in air, even at low temperatures.

Based on the high thermal stability of our AGO, the isothermal thermogravimetric behavior was investigated by varying the isothermal heat-treatment temperature and duration to assess the possibility of the thermal reduction of AGO in air. After heating to 175 °C, thermal deoxygenation occurred for 10 min, resulting in a weight loss of 10%. The subsequent heating (200 °C) and isothermal treatment resulted in the rapid deoxygenation of AGO. XPS analysis reveals that large amounts of hydroxyl or epoxy groups were removed from AGO above 200 °C, as shown in Fig. 4a. Interestingly, the deoxygenation of

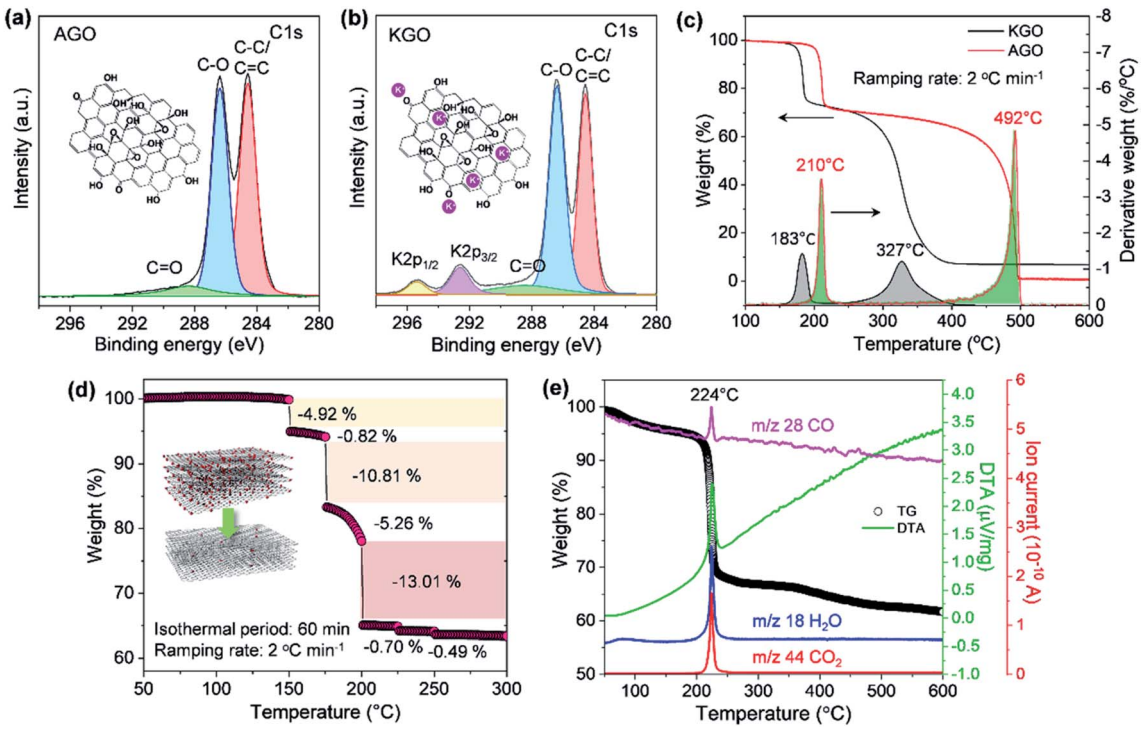

Fig. 3 C 1s XPS spectra of (a) AGO and (b) KGO. (c) TGA results for AGO and KGO in air. (d) Isothermal thermogram in air for AGO at 150, 175, 200, 225, and 250 °C for 60 min; the ramping rate at each step is 2 °C min^{-1}. (e) TGA-MS data of AGO under an Ar environment showing H_2O (*m*/*z* 18), CO (*m*/*z* 28), and CO_2 (*m*/*z* 44).

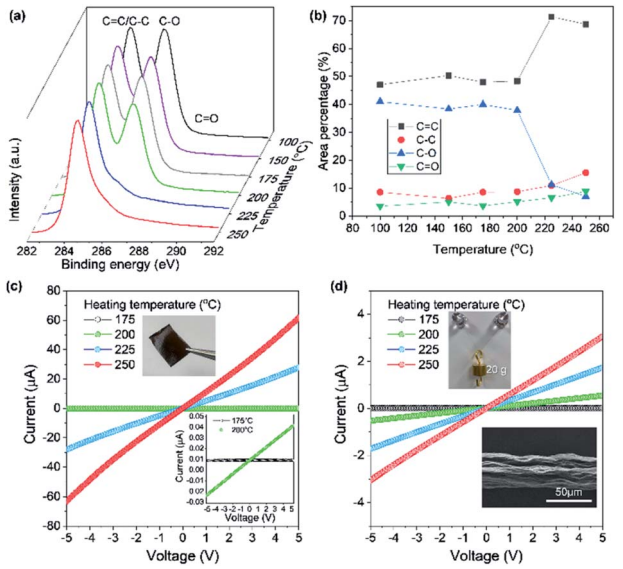

Fig. 4 Chemical structures and electrical properties of AGO samples after thermal treatment in air: (a) C 1s XPS spectra and (b) atomic area percentage of AGO films after thermal treatment in air for 1 h. *I*–*V* plots of (c) AGO films and (d) AGO fibers after thermal treatment in air for 1 h. The upper photo image in (c) and (d) shows the AGO film and fiber, respectively. The lower image in (d) shows the FE-SEM image of the AGO fiber.

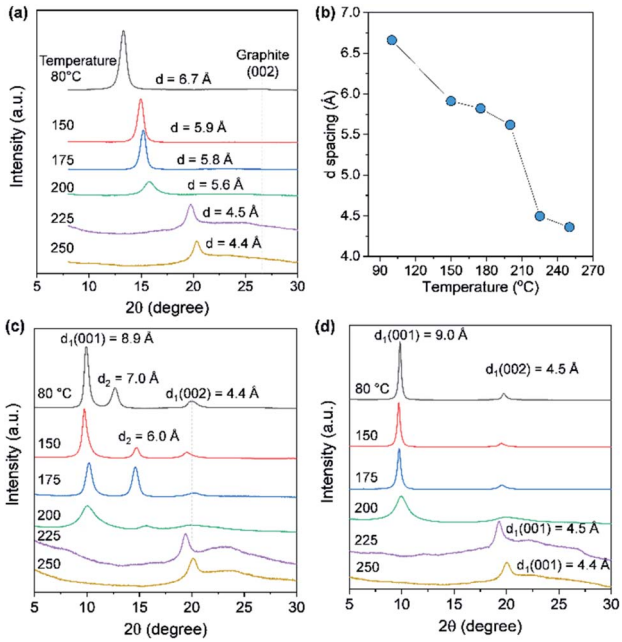

Fig. 5 (a) X-ray diffraction patterns and (b) *d*-spacing of AGO films upon thermal treatment at different temperatures for 1 h. (c and d) XRD patterns of thermally treated AGO films after immersing in EtOH for (c) 3 h and (d) 15 h.

the densely packed AGO films occurred above 200 °C, while in the TGA experiment, the freeze-dried AGO samples were readily and drastically deoxygenated, even at 200 °C. This result indicates that oxidative molecules from the less defective AGO film tend to be removed at more elevated temperatures. This deoxygenation process was elucidated by thermally deoxygenating AGO films and fibers to recover the sp^2 domain. AGO fibers were fabricated by solution spinning with 1.4 wt% AGO solution and using acetone as the coagulation bath. Solution-cast AGO films have a densely packed structure, while the solution-spun AGO fibers display micrometer-scale roughness. Fig. 4c shows the *I*–*V* plots of the AGO films obtained for various heating temperatures in air. The electric current flow of the densely packed AGO film was increased slightly at 200 °C, whereas it increased dramatically above 200 °C. However, porous AGO fibers were more electrically conductive than the AGO films after treatment at 200 °C. This result corresponds to the difference between the TGA results of the freeze-dried AGO powder and the XPS results of the solution-cast AGO films that exhibit barrier properties. Moreover, this result is in stark contrast to the electrical properties of thermally reduced GO films synthesized by $KMnO_4$-based oxidation having defective basal plane structures and highly oxidized functional groups (Fig. S4b†).

The *d*-spacing of solution-cast AGO films with a thickness of 5 μm was measured by XRD to further investigate the barrier properties of the thermally treated AGO films. As shown in Fig. 5a and b, the *d*-spacing of the (001) GO plane was decreased upon increasing the temperature due to the evaporation of water molecules and then decreased dramatically for temperatures greater than 200 °C, reaching 4.4 Å at 250 °C due to deoxygenation, in agreement with the XPS results presented in Fig. 4a. The reduced AGO films were immersed in ethanol, and then the second (001) peak was generated, which is indicative of the swelling of AGO films. However, AGO treated at temperatures above 225 °C was stable, even after immersing for 15 h, while the *d*-spacing of the AGO films treated at temperatures below 200 °C increased to 9 Å. Moreover, to investigate the water barrier properties, the WVTR of the GO films with a thickness of 1 μm on the polyimide (PI) film were measured by the MOCON method. The WVTR of PI decreased from 43.7 to 25.7 g m^{-2} day after the deposition of the AGO layer, while the $KMnO_4$-based GO layer did not act as a barrier layer after thermal deoxygenation at 175 °C (Fig. S5†). These results indicate the less defective basal plane structure of the prepared AGO nanosheets.

Conclusions

Herein, we demonstrated a rational approach for preparing thermally stable GO nanosheets by exfoliating GO fabricated using the modified Brodie method in an ammonia solution. TGA revealed that AGO was stable even at 200 °C, and deoxygenated dramatically at 210 °C and a heating rate of 2 °C min^{-1}, even in air. This is in stark contrast to the thermal behavior of the GO prepared by $KMnO_4$-based oxidation and GO containing metal ions. The AGO films and fibers became electrically conductive after thermal reduction in air at ~200–250 °C. Thus, a comprehensive analysis of the GO synthesized in this work may provide a synthetic pathway to high-quality GO. The superior thermal stability of the GO obtained in this work is due to the absence of the metal ions that facilitate thermal

decomposition and highly oxidative functional groups, such as carboxyl and lactol groups that possess defective basal plane structures. Our work makes several critical contributions: (i) this is the first study to prepare thermally stable graphene oxide after deoxygenation in air and (ii) demonstrates the fabrication of reduced graphene oxide by thermal reduction of GO at low temperatures, even in air with the formation of films and fibers as electrodes.

Conflicts of interest

There are no conflicts to declare.

Acknowledgements

This research was supported by the Primary Research Program (21A01002) of the Korea Electrotechnology Research Institute.

References

1 J. Zhao, S. Pei, W. Ren, L. Gao and H.-M. Cheng, *ACS Nano*, 2010, **4**, 5245.
2 E. J. Yoo, T. Okata, T. Akita, M. Kohyama, J. Nakamura and I. Honma, *Nano Lett.*, 2009, **9**, 2255.
3 G. Yu, L. Hu, M. Vosgueritchian, H. Wang, X. Xie, J. R. McDonough, X. Cui, Y. Cui and Z. Bao, *Nano Lett.*, 2011, **11**, 2905.
4 Y. Fu, L. Liu, J. Zhang and W. C. Hiscox, *Polymer*, 2014, **55**, 6381.
5 S. Zhou and A. Bongiorno, *Sci. Rep.*, 2013, **3**, 2484.
6 N. Ghaderi and M. Peressi, *J. Phys. Chem. C*, 2010, **114**, 21625.
7 Y. Yamada, K. Murota, R. Fujita, J. Kim, A. Watanabe, M. Nakamura, S. Sato, K. Hata, P. Ercius, J. Ciston, C. Y. Song, K. Kim, W. Regan, W. Gannett and A. Zettl, *J. Am. Chem. Soc.*, 2014, **136**, 2232.
8 D. C. Marcano, D. V. Kosynkin, J. M. Berlin, A. Sinitskii, Z. Sun, A. Slesarev, L. B. Alemany, W. Lu and J. M. Tour, *ACS Nano*, 2010, **4**, 4806.
9 S. Seiler, C. E. Halbig, F. Grote, P. Rietsch, F. Börrnert, U. Kaiser, B. Meyer and S. Eigler, *Nat. Commun.*, 2018, **9**, 836.
10 J. Y. Cho, J. I. Jang, W. K. Lee, S. Y. Jeong, J. Y. Hwang, H. S. Lee, J. H. Park, S. Y. Jeong, H. J. Jeong, G. W. Lee and J. T. Han, *Carbon*, 2018, **138**, 219.
11 A. Y. S. Eng, C. K. Chua and M. Pumera, *Nanoscale*, 2015, **7**, 20256.
12 S. Y. Jeong, S. H. Kim, J. T. Han, H. J. Jeong, S. Y. Jeong and G.-W. Lee, *Adv. Funct. Mater.*, 2012, **22**, 3307.
13 X. Fan, W. Peng, Y. Li, X. Li, S. Wang, G. Zhang and F. Zhang, *Adv. Mater.*, 2008, **20**, 4490.
14 D. Marx, A. Chandra and M. E. Tuckerman, *Chem. Rev.*, 2010, **110**, 2174.
15 F. Kim, J. Luo, R. Cruz-Silva, L. J. Cote, K. Sohn and J. Huang, *Adv. Funct. Mater.*, 2010, **20**, 2867.
16 S. Y. Jeong, S. H. Kim, J. T. Han, H. J. Jeong, S. Yang and G.-W. Lee, *ACS Nano*, 2011, **5**, 870.
17 J. Y. Cho, J. H. Kim, H. J. Yang, J. H. Park, S. Y. Jeong, H. J. Jeong, G. W. Lee and J. T. Han, *Carbon*, 2020, **157**, 663.
18 C. Botas, P. Álvarez, P. Blanco, M. Granda, C. Blanco, R. Santamaría, L. J. Romasanta, R. Verdejo, M. A. López-Manchado and R. Menéndez, *Carbon*, 2013, **65**, 156.